Article:

Zhao, Xing orcid.org/0000-0003-4000-0446, Wang, Sigao, Niu, Shuangxia et al. (2 more authors) (2022) A Novel High-order-harmonic Winding Design Method for Vernier Reluctance Machine with DC Coils across Two Stator Teeth. IEEE Transactions on Industrial Electronics. pp. 7696-7707. ISSN 0278-0046

https://doi.org/10.1109/TIE.2021.3104589

A Novel High-Order-Harmonic Winding Design Method for Vernier Reluctance Machine with DC Coils across Two Stator Teeth

Xing Zhao, *Member, IEEE*, Sigao Wang, Shuangxia Niu, *Senior Member, IEEE,* Weinong Fu, Xiaodong Zhang

***Abstract*—Vernier reluctance machine (VRM) with DC field coils in stator is a competitive rare-earth-free design for variable-speed industrial applications due to its robust structure and controllable excitation, while its torque density is relatively disadvantageous. To address this issue, this paper proposes a new armature winding design method for VRM with DC field coils across two stator teeth. The key is to break the traditional winding design principle based on the flux modulation effect of fundamental DC field harmonic, and instead, reconstruct a novel harmonic winding to enhance the utilization factor of the modulated high-order DC field harmonics arising from the unique magnetomotive force distribution of DC field coils across two stator teeth. By this means, the torque density can be improved by 75.6% compared to the existing counterpart. In this paper, the machine structure and operation principle are introduced, with emphasis on the high-order DC field harmonics distribution rule and its influence on the armature winding design. By finite element design and optimization, a comparative study is performed to evaluate the electromagnetic performance of VRMs using two different winding configurations with variable slot pole combinations. A prototype is fabricated and tested, and the results agree well with finite element analysis, which verifies the feasibility and advantages of the proposed winding design method.**

***Index Terms*—Flux modulation, high-order-harmonic winding, torque density, Vernier reluctance machine.**

I. INTRODUCTION

DUE to a limited resource of rare-earth PM material and the associated price fluctuation, the system cost of permanent magnet machines show a significant growth in the recent years. Therefore, developing new reluctance machines without using permanent magnets (PM) becomes a hot research topic [1-4]. The synchronous reluctance machine is a promising non-PM candidate which share the same stator design and drive circuit with traditional PM machines, but its torque density and power factor are unsatisfactory [5-6]. Besides, the mechanical strength of magnetic barrier rotor is relatively weak, which restricts its industry applications. Some other types of reluctance machines employing a doubly salient structure present better mechanical robustness, including the switched reluctance machine (SRM), doubly-fed doubly salient machine (DF-DSM) and variable flux reluctance machine (VFRM). The state of art of these doubly salient topologies is provided as follows.

SRM has been well investigated in literature for many years and thus its design, modeling and control methods are relatively mature [7-9]. Nevertheless, the industrial applications of SRM are still limited. On one hand, the torque ripple of SRM is serve due to half-period-conducting principle, which leads to distinct mechanical vibration and noise. On the other hand, the drive circuit for SRM is an asymmetry half-bridge converter, thus the commercialized inverter package cannot be applied. To address this issue, a six-phase SRM with armature winding connected with diodes, is proposed to enable inverter driven feature [10], while the feasibility of slot pole design is reduced.

DF-DSM shares a similar stator and rotor structure with SRM but equipped with extra DC field coils in stator core. Benefiting from the DC field coils, an alternating excitation flux linkage is established, which enables DF-DSM to work in a whole period. Hence, DF-DSM can be driven by a universal inverter package [11-12]. The main issue of DF-DSM that limits its applications is the large torque ripple, caused by the asymmetrical magnetic circuit [13], rich even-order flux harmonics and the associated distorted back electromotive force (EMF) [14-15].

VFRM can be considered as a special DF-DSM by changing the layout of DC coils to create a more uniform magnetomotive force and thus enables more flexible slot pole designs [16-17]. Especially, VFRM with odd rotor poles in unit machine design shows distinctly reduced torque ripple compared to DF-DSM, due to symmetrical magnetic circuit, eliminated even-order flux harmonics and constant phase inductance [18]. Considering the inverter-driven feature and low torque ripple, VFRM is a good non-PM candidate for industrial applications. The bottleneck of VFRM is low torque density. In the recent years, it is revealed VFRM operates based on the flux modulation principle and thus can be referred as Vernier reluctance machine (VRM) [19-20]. To improve the torque density of VRM, integrated armature and field current control can be applied using zero-sequence current injection to eliminate the space conflict between AC coils and DC coils [21-23]. However, the dual inverter should be adopted, which increases the complexity of drive circuit.

VRMs with DC coils across two stator teeth is an emerging non-PM candidate. Compared to DF-DSM, it has symmetrical magnetic circuit and sinusoidal back EMF, which contributes to reduced torque ripple [24-26]. Compared to the traditional VRMs using full DC coils, it shows comparable torque density but with reduced DC coils and the associated DC copper loss. In general, VRMs with DC coils across two stator teeth, can be a potential non-PM topology that integrates both small torque ripple and acceptable efficiency, while its torque density (about 5kNm/m^3 [27-28]) needs to be further improved for industrial applications. The reasons for low torque density of existing VRM structures include: (1) The flux linkage in each armature coil is biased, thus the stator core utilization factor is relatively

Manuscript received xxxx, 2021; This work was supported by the Project No. 152509/16E under the Research Grant Council, Hong Kong SAR, and the Project No. 51707171 under National Natural Science Foundation of China.

Xing Zhao, Sigao Wang, Shuangxia Niu and Weinong Fu are with the Department of Electrical Engineering, Hong Kong Polytechnic University. Xiaodong Zhang is with the School of Professional Education and Executive Development, Hong Kong Polytechnic University, Hong Kong SAR, China.

low. (2) Some working harmonics in the air gap are not fully utilized when using the traditional winding design method.

In this paper, a novel armature winding design method will be proposed to improve the torque density of VRMs with DC coils across two stator teeth. The key is to break the traditional winding design principle based on the flux modulation effect of fundamental harmonic of excitation source, and instead, design a novel high-order harmonic winding according to the unique distribution of magnetomotive force excited by DC coils across two stator teeth, thus achieve enhanced flux modulation effect to boost torque density. The rest of paper is organized as follows. In Section II, the machine structure, armature winding designs, and operation principle are introduced by harmonics analysis based on a magnetomotive-force-permeance analytical model. In Section III, the Genetic Algorithm (GA) is used to perform multi-objective design and optimization for VRMs considering different winding design methods and slot pole combinations. In Section IV, the optimal cases are comprehensively compared in terms of the flux linkage, back EMF, torque performance, loss, efficiency, power factor, as well as radial magnetic force. In Section V, a prototype is fabricated, and the experiments are performed for the feasibility verification of proposed solution. Finally, some conclusions are drawn in Section VI.

II. MACHINE STRUCTURE AND WORKING PRINCIPLE

A. Machine structure and winding designs

The configuration of Vernier reluctance machine (VRM) to be analyzed is presented in Fig.1. There are 12 stator slots and 11 rotor poles. The rotor consists of iron core only and hence shows good mechanical robustness. There are two groups of windings in the stator slots, namely DC field winding and AC armature winding, respectively. The DC field coils are wound across every two stator teeth, which will produce abundant field harmonics including the fundamental field harmonic and other high order components. How to design an AC armature winding to achieve the highest utilization factor of DC field harmonics, becomes an interesting topic in this VRM topology.

Two feasible designs of AC armature winding are discussed in this paper. One is the traditional winding configuration that is designed based on the flux modulation effect of fundamental DC field harmonic, which can be expressed as

$$PPN_a = \left|N_p - N_r\right| \tag{1}$$

where PPN_a is the pole pair number (PPN) of AC armature winding, N_r is the number of rotor salient poles, and N_p is the *PPN* of fundamental harmonic of DC field excitation. The other new armature winding design is proposed according to the flux modulation effect of high-order DC field harmonics, especially the rich components modulated from the third-order DC field harmonic component excited by the unique distribution of DC field coils across two stator teeth, which will be expanded in the Part B. The design principle of proposed high-order-harmonic armature winding can be expressed as

$$PPN_a = \left|3N_p - N_r\right| \tag{2}$$

Using the case of 12 stator slots and 11 rotor pole pairs, detail connections of two winding designs based on equations (1) and (2) are presented in Fig. 2(a) and Fig. 2(b), respectively.

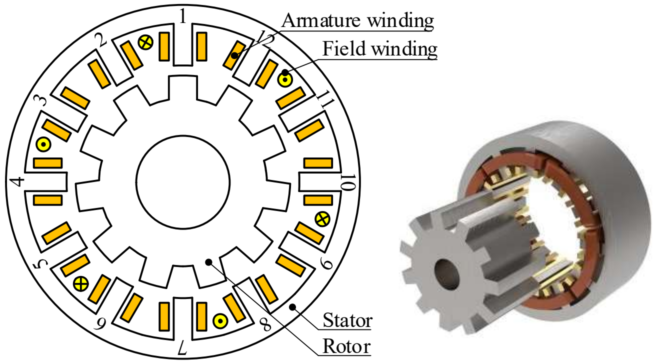

Fig. 1. Structure of 12/11 VRM with DC field coils across two stator teeth.

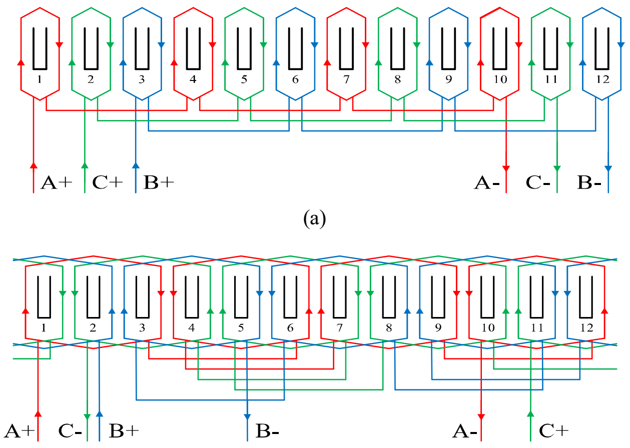

(a)

(b)

Fig. 2. Connections of AC armature winding. (a) The traditional fundamental-harmonic design. (b) The proposed high-order-harmonic design.

B. Distribution rule of DC field harmonics

To provide a deep understanding of the proposed winding design method, it is necessary to analyze the distribution rule of DC field harmonics in air gap. In this paper, a simple air-gap magnetomotive force (MMF) and permeance analytical model is utilized to calculate the air-gap flux density and determine the harmonics distribution [27].

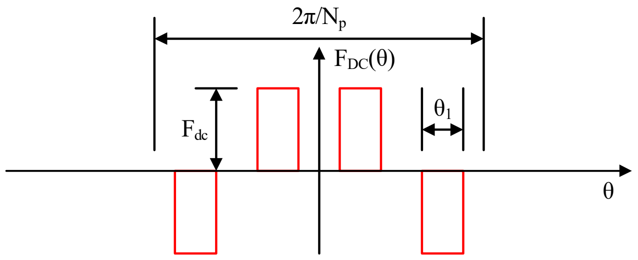

Fig. 3. MMF waveform generated by DC field excitation.

Fig. 3 presents the MMF waveform with respective to mechanical angle generated by DC field coils across two stator teeth. The amplitude of MMF waveform under every stator tooth is the same due to magnetic circuit symmetry, and the polarity of MMF is changed every two teeth. Therefore, it can be further expanded by means of Fourier Series as

$$\begin{cases} F_{DC}(\theta)=\sum_{n=1}^{+\infty} F_n \cos(nN_p\theta) \\ F_n = \dfrac{4F_{dc}}{n\pi}\sin\left(n\dfrac{N_p}{2}\theta_1\right)\left[\cos\left(\dfrac{n\pi}{4}\right)-\cos\left(\dfrac{3n\pi}{4}\right)\right] \end{cases} \quad (3)$$

where F_{dc} is the equivalent MMF of DC field current, θ is the mechanical angle, θ_1 is the mechanical angle of the stator tooth.

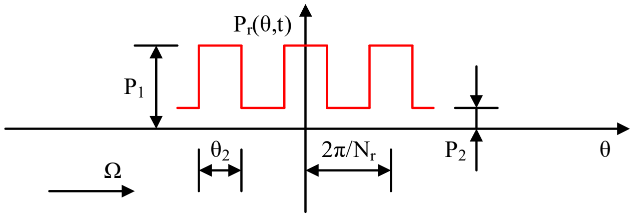

Fig. 4. Rotor permeance waveform.

Fig. 4 presents the rotor permeance that is modulated by rotor slots and salient poles, and it can be expanded as

$$\begin{cases} P_r(\theta,t)=\dfrac{P_0}{2}+\sum_{k=1}^{+\infty} P_k \cos[kN_r(\theta-\omega_{me}t)] \\ P_0 = 2P_2+\dfrac{(P_1-P_2)\theta_2 N_r}{\pi} \\ P_k = \dfrac{2}{k\pi}(P_1-P_2)\sin\left(kN_r\dfrac{\theta_2}{2}\right) \end{cases} \quad (4)$$

where P_1 is the permeance of rotor salient poles, and P_2 is the permeance of rotor slots, N_r is the number of rotor salient poles, ω_{me} is the mechanical angular speed of the rotor, θ_2 is the mechanical angle of the rotor salient pole.

The air-gap flux density can be deduced by multiplying (3) and (4), and be further expressed as:

$$B_r(\theta,t)=F_{DC}(\theta)P_r(\theta,t)=\sum_{n=1}^{+\infty}\sum_{k=-\infty}^{+\infty}\frac{F_nP_{|k|}}{2}cos(nN_p\theta+kN_r\theta-kN_r\omega_{me}t) \quad (5)$$

TABLE I

DISTRIBUTION OF AIR-GAP DC FIELD HARMONICS

Group Number	Pole Pair Number	Rotating Speed
I	N_pn	0
II	N_pn+N_rk	$\dfrac{N_rk}{N_pn+N_rk}\omega_{me}$
III	$\lvert N_pn-N_rk\rvert$	$\dfrac{N_rk}{\lvert N_pn-N_rk\rvert}\omega_{me}$

The PPN of each harmonic component and its rotation speed can be summarized in Table I based on the result in (5). There are three groups of modulated air-gap harmonics. The harmonic components in Group I are corresponding to the case when $k=0$. They are not modulated by the rotor salient poles and instead established directly from DC field current. They have zero rotation speed, which means they cannot be utilized as working harmonics. The harmonic components in Group II are related to the cases when k is positive number, and the Group III is corresponding to the cases when k is negative. The harmonics in Group II and III are modulated by the rotor salient poles, and some of them can be utilized as working harmonics.

C. Selection of the main working harmonics

For the traditional design method of AC armature winding, the main working harmonic is selected as the component which is modulated from the fundamental DC field harmonic (*PPN* of $|N_p\text{-}N_r|$, with n=1, k=-1), while for the proposed design method, the main working harmonic is determined as the one modulated from the third-order DC field harmonic (*PPN* of $|3N_p\text{-}N_r|$, with n=3, k=-1). Further, to explain the reasonability of the proposed high-order-harmonic winding design method, the ratio of flux density amplitudes of the above two working harmonics can be derived out by (5) and expressed as follows

$$\left|\frac{B_{(1,-1)}}{B_{(3,-1)}}\right| = \left|\frac{F_1P_{|-1|}}{F_3P_{|-1|}}\right| = \left|\frac{\dfrac{4F_{dc}}{\pi}sin\left(\dfrac{N_p}{2}\theta_1\right)\left[cos\left(\dfrac{\pi}{4}\right)-cos\left(\dfrac{3\pi}{4}\right)\right]}{\dfrac{4F_{dc}}{3\pi}sin\left(3\dfrac{N_p}{2}\theta_1\right)\left[cos\left(\dfrac{3\pi}{4}\right)-cos\left(\dfrac{9\pi}{4}\right)\right]}\right| = \left|\frac{3sin\left(\dfrac{N_p}{2}\theta_1\right)}{sin\left(\dfrac{3N_p}{2}\theta_1\right)}\right| \quad (6)$$

where $B_{(1,-1)}$ and $B_{(3,-1)}$ refer to the flux density amplitude of the main working harmonic in the traditional design method and the proposed design method, respectively. It is interesting to find that the result is related to the PPN of DC field excitation N_p and the mechanical angle of stator tooth θ_1, but independent of the number of rotor salient poles N_r.

Assuming the mechanical angle of stator tooth is in close to that of the adjacent stator slot opening, which means

$$\theta_1 \approx \frac{\pi}{4N_p} \quad (7)$$

By substituting (7) into (6), the ratio between two main working harmonics can be calculated as

$$\left|\frac{B_{(1,-1)}}{B_{(3,-1)}}\right| = \left|\frac{3sin\left(\dfrac{N_p}{2}\theta_1\right)}{sin\left(\dfrac{3N_p}{2}\theta_1\right)}\right| \approx 1.24 \quad (8)$$

The result in (8) indicates, regardless of the number of the rotor salient poles, the ratio between $B_{(1,-1)}$ and $B_{(3,-1)}$ is always in close to 1.24. This is because the flux density of main working harmonics is mainly determined by the fundamental waveform of DC field excitation. Because of the unique distribution of DC field coils across two stator teeth in the proposed VRMs, the flux density amplitude of the $|N_p - N_r|$ order harmonic and the $|3N_p - N_r|$ order harmonic are very close, which provides more design feasibility in the proposed VRMs to reselect the main working harmonic and boost torque density. Specifically, we propose a new $|3N_p - N_r|$ winding design method to reselect the high-order harmonics as the main working harmonics in VRM structures. Because the reselected main working harmonic has higher rotating speed, enhanced back EMF and torque generation can be achieved. The detail analysis of harmonics contribution on back EMF will be expanded in the Part E. Overall, the proposed winding design method breaks the traditional $|N_p - N_r|$ winding design principle based on the flux modulation theory of fundamental harmonic, and thus provides more feasible slot pole combinations and winding design choices.

It should be pointed out, when the similar MMF analysis is applied to VRMs with DC field coils fully wound on every stator tooth, the ratio between $B_{(1,-1)}$ and $B_{(3,-1)}$ can be derived out as 3. In other words, the flux density amplitude of $|3N_p\text{-}N_r|$ order harmonic is much smaller compared to that of $|N_p - N_r|$ order harmonic. Hence, the proposed winding design method is not recommended for VRMs with full DC field coils.

TABLE II
PPN OF ARMATURE WINDING USING DIFFERENT DESIGNS

N_{slot}	N_r	PPN of the traditional $\lvert N_p - N_r\rvert$ winding	PPN of the proposed $\lvert 3N_p - N_r\rvert$ winding
12	11	8	2
12	10	7	1
12	8	5	1
12	7	4	2

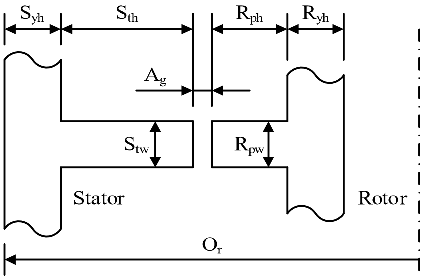

Fig. 5. Notations of dimensional parameters.

TABLE III
DIMENSION PARAMETERS OF INITIAL DESIGN

Item	Notation	Value
Stack length (mm)	L_{st}	50
Outer radius (mm)	O_r	70
Stator tooth width (mm)	S_{tw}	8
Stator tooth height (mm)	S_{th}	20
Stator yoke height (mm)	S_{yh}	9
Air gap length (mm)	A_g	0.5
Rotor pole height (mm)	R_{ph}	10
Rotor yoke height (mm)	R_{yh}	20
Rotor pole width (mm)	R_{pw}	9
Number of turns of DC field coil	N_{DC}	126
Number of turns of AC armature coil	N_{AC}	96
Rotation speed (rpm)	S_{pd}	900
DC current (A)	I_{DC}	5.34

D. *Example cases and initial FEA validation*

This part shows the example cases with finite element models to validate the above-mentioned analysis of airgap harmonic distribution. In the example cases, four slot pole designs with N_{slot}/N_r of 12/11, 12/10, 12/8 and 12/7 are considered to validate the flux density ratio between $B_{(1,-1)}$ and $B_{(3,-1)}$. Based on (1) and (2), the PPN of corresponding armature winding in four cases using two different design methods are presented in Table II. Some common dimension parameters of four initial designs are labeled in Fig. 5, and their values are given in Table III. The calculated airgap harmonics distribution of four cases are presented in Fig. 6, including the flux density waveforms and the associated harmonics spectrum obtained by Fast Fourier Analysis. The main working harmonic to be used in two different winding configurations are further highlighted in marked in red and blue color, respectively.

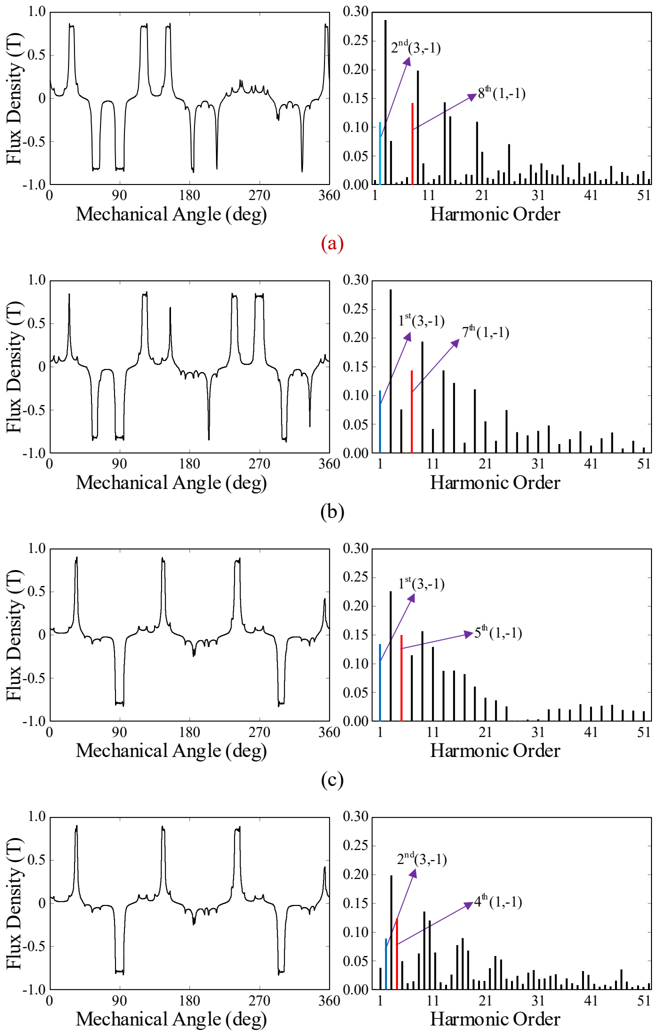

(a)

(b)

(c)

(d)

Fig. 6. Air-gap field and harmonics of VRMs. (a) 11 rotor salient poles. (b) 10 rotor salient poles. (c) 8 rotor salient poles. (d) 7 rotor salient poles.

With their flux density amplitudes listed in Table IV, it can be found that the ratio between $B_{(1,-1)}$ and $B_{(3,-1)}$ is 1.30 for 12/11 case, 1.32 for 12/10 case, 1.12 for 12/8 case, 1.39 for 12/7 case, respectively. This basically agrees with the result from theoretical analysis in (8) considering the mechanical angle of stator tooth is not exactly the same with slot opening angle.

TABLE IV
AMPLITUDES OF MAIN WORKING HARMONICS

N_{slot}	N_r	$B_{(1,-1)}$ (T)	$B_{(3,-1)}$ (T)	$\left\lvert\frac{B_{(1,-1)}}{B_{(3,-1)}}\right\rvert$
12	11	0.142	0.109	1.31
12	10	0.144	0.109	1.32
12	8	0.150	0.134	1.12
12	7	0.123	0.089	1.39

E. *Quantitative analysis of harmonics contribution*

The following part gives the analytical relation between open-circuit back EMF and working harmonics with two winding designs. The amplitude of back EMF is in direct proportion to torque production if core saturation is not considered, and the back EMF can be expressed as:

TABLE V

OPEN-CIRCUIT BACK EMF CONTRIBUTION FROM DIFFERENT HARMONICS IN 12/11/8 MODEL

Order	(n,k)	B_n (T)	ω_n	k_{pn}	k_{dn}	k_{wn}	$B_n\omega_n k_{wn}$	$\Sigma B_n\omega_n k_{wn}$
2	(3,-1)	0.1093	$11\omega_{me}/2$	0.5	0	0	0	$0.3072\omega_{me}$
4	(5,-1)	0.0755	$11\omega_{me}/4$	0.866	1	0.866	$0.1798\omega_{me}$	
8	(1,-1)	0.1419	$11\omega_{me}/8$	0.866	1	0.866	$0.1690\omega_{me}$	
10	(7,-1)	0.0376	$11\omega_{me}/10$	0.5	0	0	0	
14	(-1,-1)	0.1433	$11\omega_{me}/14$	-0.5	0	0	0	
16	(9,-1)	0.007	$11\omega_{me}/16$	-0.866	1	-0.866	$-0.004\omega_{me}$	
20	(-3,-1)	0.1096	$11\omega_{me}/20$	-0.866	1	-0.866	$-0.0522\omega_{me}$	
22	(11,-1)	0.0114	$11\omega_{me}/22$	-0.5	0	0	0	
26	(-5,-1)	0.0704	$11\omega_{me}/26$	0.5	0	0	0	
28	(13,-1)	0.0198	$11\omega_{me}/28$	0.866	1	0.866	$0.0067\omega_{me}$	
32	(-7,-1)	0.0370	$11\omega_{me}/32$	0.866	1	0.866	$0.0110\omega_{me}$	

TABLE VI

OPEN-CIRCUIT BACK EMF CONTRIBUTION FROM DIFFERENT HARMONICS IN 12/11/2 MODEL

Order	(n,k)	B_n (T)	ω_n	k_{pn}	k_{dn}	k_{wn}	$B_n\omega_n k_{wn}$	$\Sigma B_n\omega_n k_{wn}$
2	(3,-1)	0.1093	$11\omega_{me}/2$	1	1	1	$0.6010\omega_{me}$	$0.5573\omega_{me}$
4	(5,-1)	0.0755	$11\omega_{me}/4$	0	0	0	0	
8	(1,-1)	0.1419	$11\omega_{me}/8$	0	0	0	0	
10	(7,-1)	0.0376	$11\omega_{me}/10$	1	1	1	$0.0413\omega_{me}$	
14	(-1,-1)	0.1433	$11\omega_{me}/14$	-1	1	-1	$-0.1125\omega_{me}$	
16	(9,-1)	0.007	$11\omega_{me}/16$	0	0	0	0	
20	(-3,-1)	0.1096	$11\omega_{me}/20$	0	0	0	0	
22	(11,-1)	0.0114	$11\omega_{me}/22$	-1	1	-1	$-0.0057\omega_{me}$	
26	(-5,-1)	0.0704	$11\omega_{me}/26$	1	1	1	$0.0298\omega_{me}$	
28	(13,-1)	0.0198	$11\omega_{me}/28$	0	0	0	0	
32	(-7,-1)	0.0370	$11\omega_{me}/32$	0	0	0	0	

$$E_{phn} = \frac{4.44 D L T_{ph}}{60}\left(B_n k_{wn} \omega_n\right) \qquad (9)$$

where D is the diameter of the airgap circumference, L is the stack length, T_{ph} is the number of turns in a phase, E_{phn} is the amplitude of back EMF contributed by nth harmonic, B_n is the amplitude of nth harmonic, k_{wn} is the winding factor of nth harmonic, and ω_n is the rotation speed of nth harmonic.

To give a quantitative analysis between the proposed and traditional winding design, the open-circuit back EMF produced by each harmonic and their amplitude, rotation speed and winding factor are calculated and listed in Table V and Table VI, where k_{pn} and k_{dn} are pitch factor and distribution factor, respectively, using 12/11/8 and 12/11/2 cases as the examples. The harmonics with the order higher than 32 can be neglected as the amplitudes of flux density are too small.

Although $B_{(1,-1)}$ has relatively higher amplitude than $B_{(3,-1)}$, the corresponding rotation speed is much lower. Therefore, the model with proposed winding design has higher back EMF than traditional counterpart. The analytical ratio of back EMF between two winding designs is 1.814, which agrees with the FEA result of 1.934 (error = 6.86%). The results for 12/10, 12/8 and 12/7 cases are similar with that of 12/11 case. Due to relatively higher rotation speed, the main working harmonic in proposed winding design can contribute higher back EMF. Under the same dimensional parameters listed in Table III, the analytical and FEA results are summarized in Table VII. It can be found the analytical results well agree with FEA results.

In general, according to the flux modulation theory, the rotation speed of modulated harmonic is in inverse proportion to harmonic order. The lower order of working harmonic is, the higher rotation speed can be achieved, which means the higher back EMF and torque production can be obtained. This is the motivation of the proposed novel winding design method.

TABLE VII

ANALYTICAL AND FEA RESULTS OF OPEN-CIRCUIT BACK EMF RATIO

N_{slot}	N_r	Analytical	FEA	Error
12	11	1.814	1.9383	6.86%
12	10	3.139	2.8997	7.63%
12	8	2.9029	2.8430	2.06%
12	7	1.7848	1.7938	0.51%

III. DESIGN OPTIMIZATION

To show the effectiveness of the proposed winding design, machines with different rotor pole pairs are firstly optimized in this part and further comparatively evaluated in the Section IV. The genetic algorithm (GA) is combined with FEA method to fast search the optimal dimension parameters for four model with rotor pole pairs of 7, 8, 10, 11, respectively. The pole pair number of 9 is not included, because this case cannot form a three-phase design using the proposed winding design method. Four models are optimized using the same outer dimension and current density, with two objectives of the maximum average torque and minimum torque ripple. The flowchart of GA and FEA combined optimization process is shown in Fig. 7.

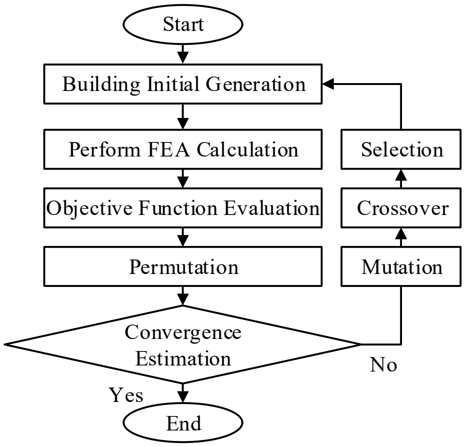

Fig. 7. Flow chart of FEA & GA optimization.

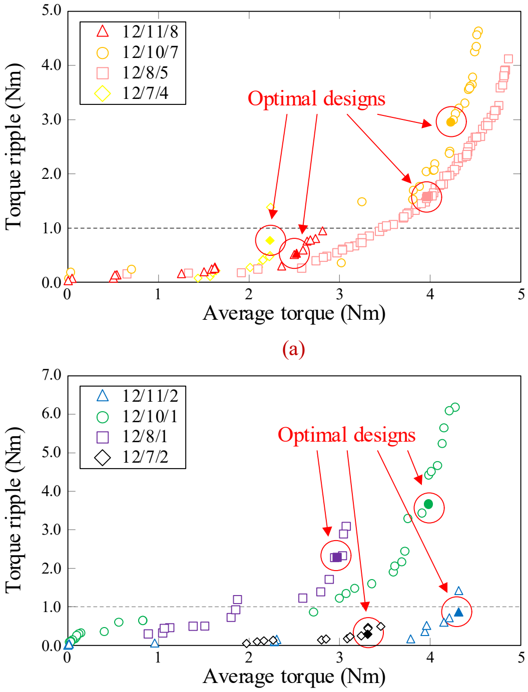

(a)

(b)

Fig. 8. Optimization results of the last generation (Pareto front). (a) Traditional $\left|N_p\text{-}N_r\right|$ winding design. (b) Proposed $\left|3N_p\text{-}N_r\right|$ winding design.

At first, to build the initial generation, a number of models are established with the same topology but different dimension parameters that are taken randomly within the given vibration range. Then, in the evaluation step, all the models are simulated under FEA to evaluate the torque performance. Further, in the selection process, a part of model is abandoned, and the rest of models are selected for the next step. Models with relatively poor torque performance has higher possibility to be abandoned. In the crossover step, the selected models exchange dimension parameters to form a new generation of models, and meanwhile, some dimensional parameters are mutated within a small range. After mutation, a new generation is built, which is supposed to have better average torque performance than the last generation. Finally, the difference between two adjacent generations will be estimated in the convergence setup, and the progress stops if the difference is smaller than the tolerance.

The common design parameters of four models include: the stack length of 50 mm, outer radius of 70 mm, air-gap length of 0.5 mm, rated speed of 900 rpm, current density of 6 A/mm^2 and slot filling factor of 0.6. After the optimization, the last generations of four models are given in Fig. 8. For each slot/pole/winding design, only one optimal model is selected, considering the tradeoff between average torque value and torque ripple. And their corresponding design data and torque performance index are listed in Table VIII and Table IX, respectively. It is shown, models using the proposed winding design method, can achieve higher maximum torque, which preliminarily proves its feasibility and technical advantage. The detail comparison of electromagnetic performance of the eight optimal models is presented in the next chapter.

TABLE VIII
OPTIMAL DIMENSIONAL PARAMETERS

	Traditional $\left|N_p\text{-}N_r\right|$ winding				Proposed $\left|3N_p\text{-}N_r\right|$ winding			
N_{slot}	12	12	12	12	12	12	12	12
N_r	11	10	8	7	11	10	8	7
PPN_a	8	7	5	4	2	1	1	2
S_{yh} (mm)	8.5	8	8.2	8.3	9	6.6	8.2	6.4
S_{th} (mm)	23.1	23.1	25.7	23.6	20	22.1	22.6	26
S_{tw} (mm)	10.1	8.3	9.9	15.7	8	9.4	6.9	11.1
R_{pw} (mm)	11.5	10.3	12	15.3	9	7.7	12.5	13.2
R_{ph} (mm)	8.4	7.5	7.6	10.5	10	11.6	8.8	9.7
R_{yh} (mm)	19.1	21.6	14.8	16.6	20	23.6	16.8	15.6
N_{DC}	126	126	126	126	126	126	126	126
N_{AC}	96	96	96	96	96	96	96	96
I_{DC} (A)	6.97	5.97	6.35	3.21	5.34	6.47	6.56	7.95
I_{AC} (A)	4.71	7.84	6.81	4.95	7.01	6.41	5.93	7.19

IV. PERFORMANCE COMPARISON OF OPTIMAL MODELS

Based on the optimal dimension parameters of each model, and considering two different winding designs, the comparison among the eight cases is presented in this chapter, including the magnetic field distribution, back electromotive force (EMF), average torque, torque ripple, loss and efficiency.

A. Flux distribution and back EMF

Among eight models, the layout of DC field winding keeps the same design with each DC coil across two stator teeth, hence the flux distribution of DC field is unchanged. The difference is caused by the AC armature winding design. Fig. 9 presents the flux distribution produced by armature winding in eight models. It can be seen, the flux path of proposed winding design is longer than that of the traditional counterpart regardless of the rotor pole number, because the PPN of the proposed $\left|3N_p\text{-}N_r\right|$ winding is lower than the traditional $\left|N_p\text{-}N_r\right|$ winding.

According to the flux modulation theory, the lower working harmonic order is, the higher the rotation speed is, and therefore higher back EMF and torque production can be obtained. It is worth pointing out that the 1-pole-pair armature field in the 12/10/1 and 12/8/1 cases is much easier to be saturated due to longer magnetic circuit, compared to that of the 2-pole-pair armature field in the 12/11/2 and 12/7/2 cases, which will limit the electromagnetic torque generation to some extent.

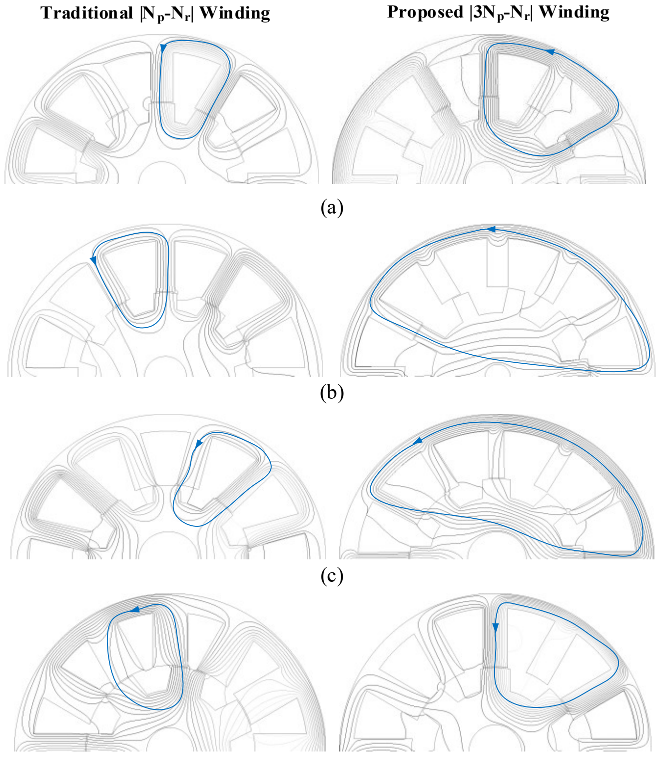

(a)

(b)

(c)

(d)

Fig. 9. Flux distribution of two different winding designs with (a) 11 rotor poles. (b) 10 rotor poles. (c) 8 rotor poles. (d) 7 rotor poles.

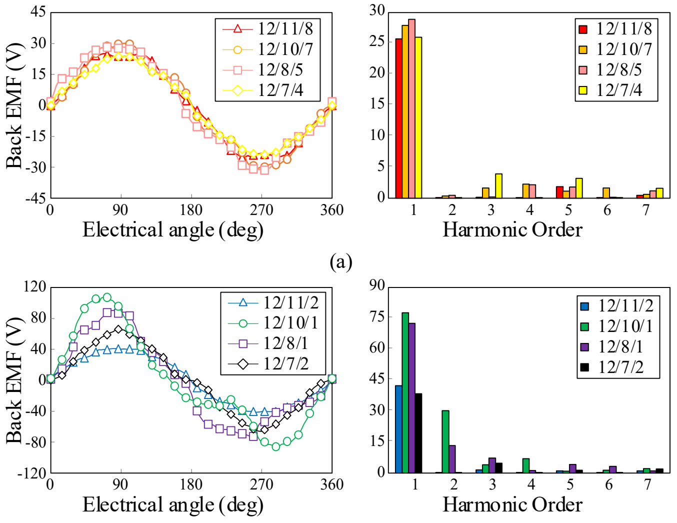

(a)

(b)

Fig. 10. Back EMF and harmonics distribution (a) Models with the traditional $|N_p\text{-}N_r|$ winding. (b) Models with the proposed $|3N_p\text{-}N_r|$ winding.

The back EMF waveforms within an electrical period at rotating speed of 900 rpm are calculated and presented in Fig. 10, along with their harmonic distribution obtained by Fast Fourier Analysis. Using the symbol of ($N_{slot}/N_r/PPN_a$) to represent each design, four models of 12/11/8, 12/10/7, 12/8/5, 12/7/4 are those having the traditional $|N_p\text{-}N_r|$ winding, while the models of 12/11/2, 12/10/1, 12/8/1, 12/7/2 employ the proposed $|3N_p\text{-}N_r|$ winding. The amplitude of back EMF of 12/11/8, 12/10/7, 12/8/5, 12/7/4 models are 25.8V, 27.9V, 28.9V, 26.0V, respectively. For 12/11/2, 12/10/1, 12/8/1, 12/7/2 models, they are 42.4V, 77.7V, 72.6V, 38.5V, respectively. This proves the effectiveness of the proposed winding, as it contributes much higher back EMF in all cases.

The total harmonic distortion (THD) of back EMF for 12/11/8, 12/10/7, 12/8/5, 12/7/4 models are calculated as 7.5%, 13.0%, 11.6%, 20.4%, respectively, while those for 12/11/2, 12/10/1, 12/8/1, 12/7/2 models are 5.7%, 40.6%, 23.0% and 13.9%, respectively. Moreover, it can be noticed that the THDs of 12/10 and 12/8 cases are relatively higher than 12/11 and 12/7 cases, because there is no even harmonics when rotor salient pole is an odd number. Overall, 12/11/2 model can achieve the enhanced back EMF and minimum THD at the same time.

B. *Torque performance*

TABLE IX
TORQUE PERFORMANCE

	N_{slot}	N_r	PPN_a	Average torque	Ripple
Traditional $\|N_p - N_r\|$ winding	12	11	8	2.45 Nm	19.8%
	12	10	7	4.19 Nm	69.2%
	12	8	5	3.96 Nm	38.4%
	12	7	4	2.24 Nm	33.2%
Proposed $\|3N_p - N_r\|$ winding	12	11	2	4.30 Nm	16.7%
	12	10	1	4.03 Nm	80.8%
	12	8	1	3.01 Nm	72.0%
	12	7	2	3.36 Nm	8.9%

The torque performance of eight models is evaluated and the results are listed in Table IX, including the average torque and torque ripple ratio, under the rated current density of 6A/mm^2. When considering the torque ripple less than 20% as a necessary condition for industry applications, designs with odd rotor pole pair are recommended. Further, the 12/11/2 case using the proposed winding design method, shows the highest average torque among all the candidates, benefiting from higher MMF utilization of DC field harmonics.

C. *Loss, efficiency, and power factor*

The core loss and efficiency of the eight models are presented in Fig. 11 and Fig. 12, respectively. The DC field current and AC armature current are fixed as the rated value, with the speed varying from 0 to 1000 rpm. It can be seen, using the proposed $|3N_p\text{-}N_r|$ winding design method, the core loss is relatively higher because of the long magnetic circuit of armature winding that makes the stator core is more saturated than the traditional models. Meanwhile, since the distributed configuration is used, the copper loss of proposed winding is also higher in this case due to the increased length of winding end. Hence, the designs using the traditional winding show relatively higher efficiency. However, the influence of end copper loss can be reduced if the machine is designed with a larger ratio of length and diameter, which is more suitable for the proposed design method.

TABLE X
COPPER LOSS UNDER RATED CURRENT

	Traditional $\|N_p\text{-}N_r\|$ winding				Proposed $\|3N_p\text{-}N_r\|$ winding			
N_{slot}	12	12	12	12	12	12	12	12
N_r	11	10	8	7	11	10	8	7
PPN_a	8	7	5	4	2	1	1	2
P_{Cu}(W)	97.89	114.03	108.92	110.21	142.98	201.92	231.7	97.51

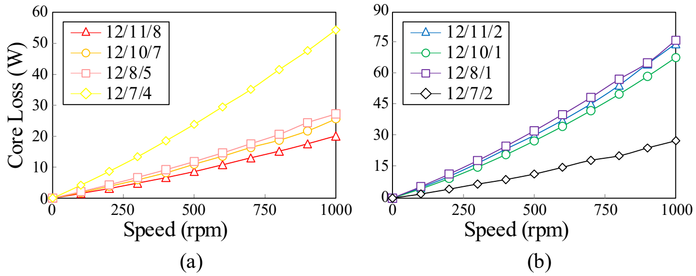

(a) (b)

Fig. 11. Core loss under rated current. (a) VRMs with traditional $|N_p\text{-}N_r|$ winding. (b) VRMs with proposed $|3N_p\text{-}N_r|$ winding.

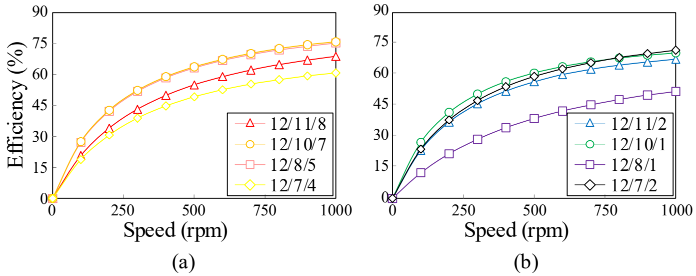

(a) (b)

Fig. 12. Efficiency under rated current. (a) VRMs with traditional $|N_p\text{-}N_r|$ winding. (b) VRMs with proposed $|3N_p\text{-}N_r|$ winding.

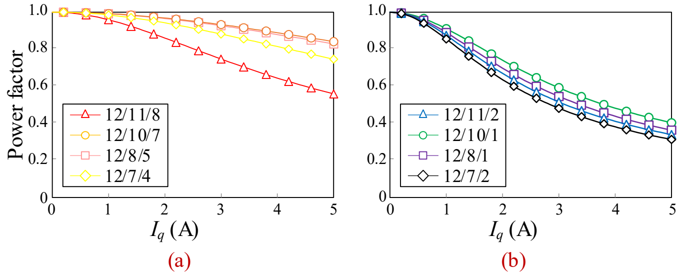

(a) (b)

Fig. 13. Power factor under different current. (a) VRMs with traditional $|N_p\text{-}N_r|$ winding. (b) VRMs with proposed $|3N_p\text{-}N_r|$ winding.

The power factor under different current of the eight models are presented in Fig. 13. It is admitted that the proposed winding design leads to relatively lower power factor than the traditional counterpart. The reason is that proposed winding designs have lower PPN than the traditional designs, therefore, distributed winding configuration is used for proposed designs, while concentrated winding configuration is used for the traditional design. Consequently, the inductance of the proposed winding design is higher, which causes stronger armature reaction and associated lower power factor.

D. Radial magnetic force

The radial magnetic force is one important factor to affect the mechanical vibration and noise in electrical machines, which should be evaluated in the proposed design as well. Fig. 14 and Fig. 15 shows the calculated radial magnetic force between the stator and rotor under no-load and load conditions, respectively.

It is validated that there is little radial magnetic force when even rotor salient pole number is adopted under both load and no-load conditions. While for 12/11/2 with proposed new AC winding, its unbalanced radial magnetic force is non-neglectable, and it is much higher under load condition than that of no-load condition. This issue should be considered during design stage. One potential solution is to use 24/22/4 design by doubling the 12/11/2 case as the unit machine design.

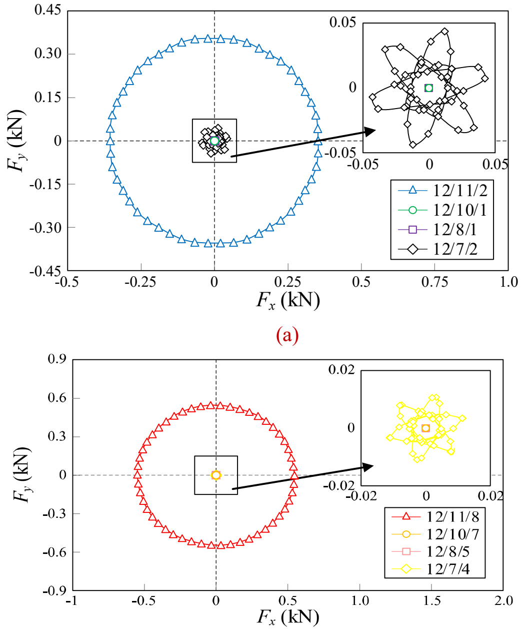

(a)

(b)

Fig. 14. Radial magnetic force under no-load condition. (a) Traditional $|N_p\text{-}N_r|$ winding design. (b) Proposed $|3N_p\text{-}N_r|$ winding design.

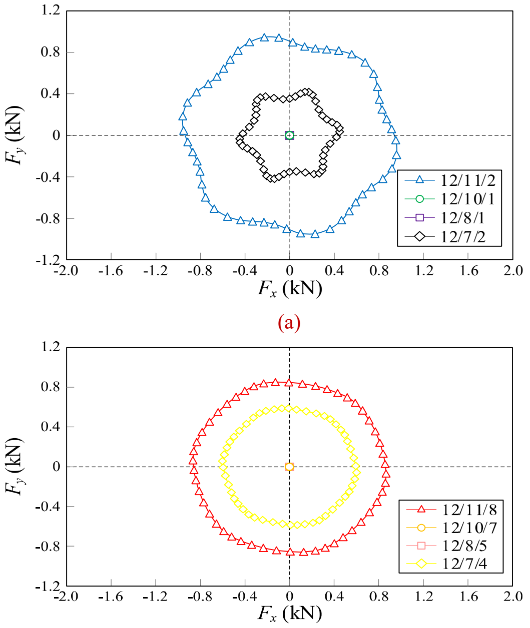

(a)

(b)

Fig. 15. Radial magnetic force under load condition. (a) Traditional $|N_p\text{-}N_r|$ winding design. (b) Proposed $|3N_p\text{-}N_r|$ winding design.

V. EXPERIMENTAL VALIDATION

In this part, a prototype of 12/11/2 design was manufactured and tested to validate the above finite element analysis. The parameters of prototype are in line with those data in Table VIII. Fig. 16 presents the manufacturing details of machine prototype and the setup of test bench, which mainly includes the magnetic powder brake, prototype, inverter, drive controller, DC power source and oscilloscope. In the testing process, the magnetic powder brake functions as a controllable load. The DC field current is provided by an independent DC power source. The traditional vector control method of AC synchronous machine can be directly applied to the proposed machine. Using the slot/pole/winding combination of 12/11/2 case in this prototype, the winding inductance has little vibration with rotor position change. Therefore, this machine can be regarded as a non-salient machine, and the traditional $I_d=0$ vector control can be used. The control block diagram is presented in Fig. 17.

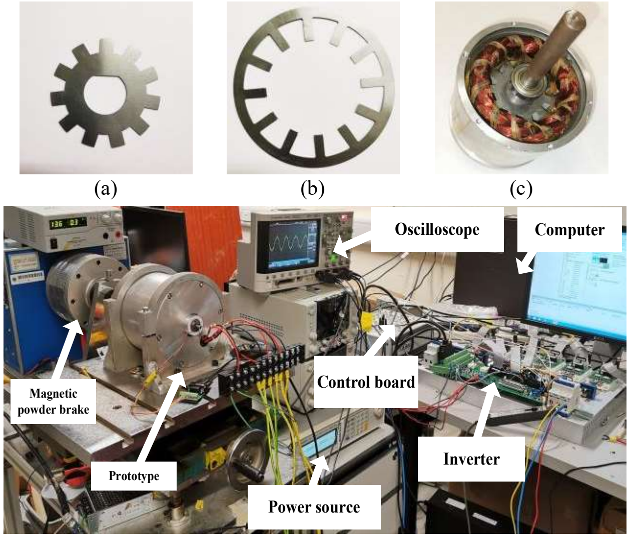
(a) (b) (c)

(d)

Fig. 16. The prototype and test bench setup. (a) Rotor core lamination (b) Stator core lamination. (c) Winding layout. (d) Test bench setup.

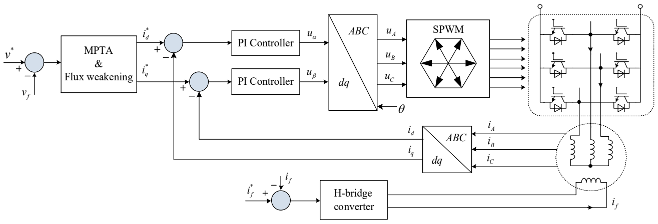

Fig. 17. Control block diagram for the prototype.

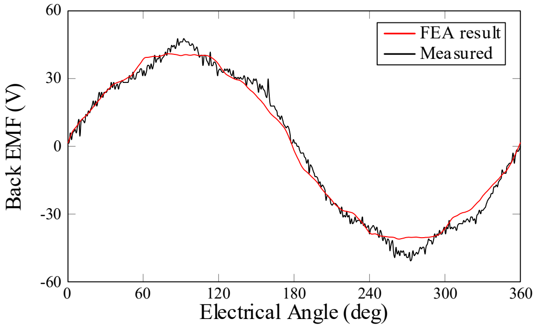

Fig. 18. Open-circuit back EMF at 900 rpm.

The open-circuit back EMF is tested at 900rpm and presented in Fig. 18. The tested result basically agrees with that of finite element analysis, while a certain distortion is observed that can be produced by mechanical fabrication tolerance. By injecting a constant DC current into armature winding and then collecting static torque at different rotor positions, the torque vs current angle curve under rated current is presented in Fig. 19, along with the FEA result. The prototype uses a salient rotor structure, but the reluctance torque makes little contribution to the overall torque production, due to the electromagnetic complementary feature of the 12/11/2 deign. Hence, maximum torque can be obtained when current angle is near 90 deg.

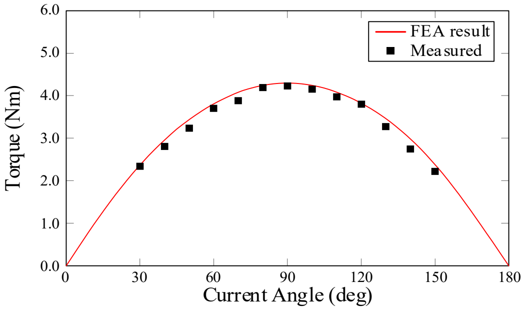

Fig. 19. Torque vs current angle curve at rated condition.

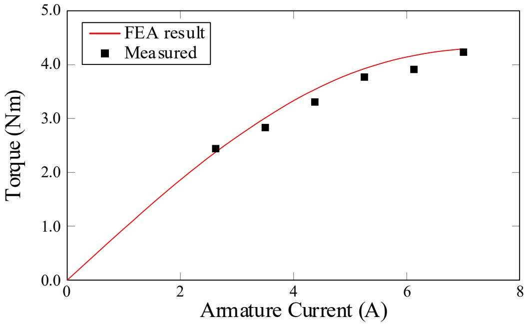

Fig. 20. Torque vs current curve, with variable AC current.

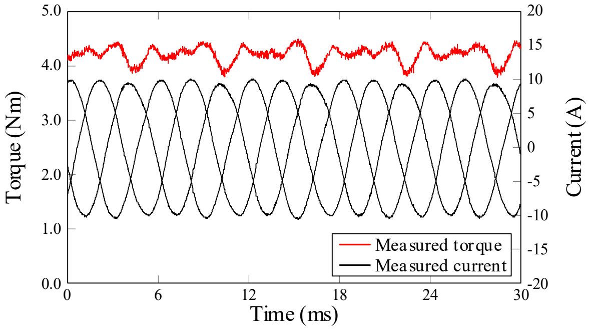

Fig. 21. Measured three-phase armature current and torque.

Further, the torque vs current curve is presented in Fig. 20, where AC current changes from zero to the rated value, while DC current keeps at the rated value all the time. Again, good agreement is achieved between testing results and FEA results. Finally, the dynamic performance is tested and given in Fig. 21. The three-phase current is measure by current sensors, while the electromagnetic torque is obtained from magnetic powder brake. The measured torque is slightly lower than the FEA predication, but it is acceptable in consideration of the error in measurement as well as mechanical fabrication tolerance.

VI. CONCLUSION

This paper proposes a novel high-order-harmonic armature winding design method for Vernier reluctance machine having DC field coils across two stator teeth, which can improve torque density by 75.6% when using 12/11 slot pole combination with